Geochemical Perspectives Letters

Growth of upper plate lithosphere controls tempo of arc magmatism: Constraints from Al-diffusion kinetics and coupled Lu-Hf and Sm-Nd chronology

E.J. Chin[1,2*], C.-T.A. Lee[1], J. Blichert-Toft[1,3]

OPEN ACCESS

doi: 10.7185/geochemlet.1503

Abstract

Most magmatism occurs at mid-ocean ridges, where plate divergence leads to decompression melting of the mantle, and at volcanic arcs, where subduction leads to volatile-assisted decompression melting in the hot mantle wedge. While plate spreading and subduction are continuous, arc magmatism, particularly in continental arcs, is characterised by >10-50 Myr intervals of enhanced magmatic activity followed by rapid decline (DeCelles *et al.*, 2009). In some cases, such as the Andes, this pattern has recurred several times (Haschke *et al.*, 2002). Abrupt changes in plate convergence rates and direction (Pilger, 1984) or repeated steepening and shallowing of subducting slabs (Kay and Coira, 2009) have been suggested as triggering flare-ups or terminating magmatism, but such scenarios may not be sufficiently general. Here, we examine the thermal history of deep crustal and lithospheric xenoliths from the Cretaceous Sierra Nevada batholith, California (USA). The deepest samples (~90 km), garnet-bearing spinel peridotites, show cooling-related exsolution of garnet from high-Al pyroxenes originally formed at >1275 °C. Modelling of pyroxene Al diffusion profiles requires rapid cooling from 1275 to 750 °C within ~10 Myr. Also suggesting deep-seated, rapid cooling is a garnet websterite from ~90 km depth with nearly identical Lu-Hf (92.6 ± 1.6 Ma) and Sm-Nd (88.8 ± 3.1 Ma) isochron ages to within error. Thermal modelling shows that this cooling history can be explained by impingement of the base of the Sierran lithosphere against a cold subducting slab at ~90 km depth, precluding cooling by shallowing subduction. Rather, the coincidence of the radiometric ages with the magmatic flare-up (120-80 Ma) suggests that the hot mantle wedge above the subducting slab may have been pinched out by magmatic (± tectonic) thickening of the upper plate, eventually terminating mantle melting. Magmatic flare-ups in continental arcs are thus self-limiting, which explains why continental arc magmatism occurs in narrow time intervals. Convective removal of the deep arc lithosphere can initiate another magmatic cycle.

Received 10 January 2015 | Accepted 13 March 2015 | Published 8 April 2015

1. Department of Earth Science, Rice University, Houston, Texas, USA
2. Department of Earth, Environmental and Planetary Sciences, Brown University, Providence, Rhode Island, USA
* Corresponding author (email: ej3030@gmail.com)
3. Ecole Normale Supérieure de Lyon and Université Lyon 1, Laboratoire de Géologie de Lyon, CNRS UMR 5276, Lyon, France

Introduction

Constraining the thermal and temporal evolution of the deep arc lithosphere is critical to understanding the magmatic evolution of a volcanic arc. The Sierra Nevada batholith is one of only a few places world-wide to study deep crustal and lithospheric evolution of an arc because of the availability of lower crustal and mantle xenoliths (Dodge *et al.*, 1988; Mukhopadhyay and Manton, 1994; Ducea and Saleeby, 1996; Lee *et al.*, 2006, 2007; Chin *et al.*, 2012), which are rare elsewhere. Magmatism in the Sierra Nevada occurred primarily between ~120 and ~80 Ma, peaking at ~95 Ma and terminating abruptly at ~80 Ma (Barton, 1996; Coleman and Glazner, 1997; Ducea, 2001; Paterson *et al.*, 2014). We examined xenoliths from a late Miocene basaltic dike (Big Creek; N 37.208946° W119.264784°) (Fig. 1A). These xenoliths comprise garnet pyroxenites and peridotites and sample a lithospheric section ranging from the mid to lower crust (~33 to ~45 km) into the mantle (~90 km) (Fig. 1B). Sm-Nd ages between 120 and 84 Ma for several pyroxenite xenoliths (Ducea and Saleeby, 1998), along with geochemical data (Lee *et al.*, 2006, 2007), indicate that they represent cumulates left behind by the Cretaceous Sierran granitoids.

Garnet pyroxenite cumulates are volumetrically dominant and can be divided into a low-MgO group composed of garnet-rich clinopyroxenites and a high-MgO group composed of garnet websterites (Lee *et al.*, 2006). The former are interpreted as mid to lower crustal cumulates of an evolved hydrous basalt, whereas the latter are lower crustal and upper mantle cumulates of primitive hydrous basalts, overlapping in final equilibration pressures and therefore interpreted as being interleaved with the spinel and garnet peridotites (Saleeby *et al.*, 2003) (Fig. 1B). Garnet-clinopyroxene rare-earth element (REE) thermobarometry of the low-MgO pyroxenite yields equilibration conditions of ~0.33 GPa and 801 °C (Sun and Liang, 2015) consistent with a mid-crustal origin. In contrast, major element thermobarometry of the high-MgO websterites record equilibration pressures ranging from 1.5 to 3 GPa and temperatures between 700 and 830 °C (Lee *et al.*, 2006). These final P-T conditions are similar to those obtained for the garnet peridotites (2.3 – 3.6 GPa, 651 – 845 °C; Chin *et al.*, 2012).

Although both garnet peridotites and high-MgO websterites achieved similar high final pressures and low final temperatures, high-Al orthopyroxene cores in both rock types point to initially high temperatures. In high-MgO websterites, orthopyroxene cores record temperatures of ~1100 °C, supporting an origin as magmatic cumulates precipitated from primary basaltic liquids (Lee *et al.*, 2006; Supplementary Information). Mineral and bulk rock compositions of the garnet peridotites indicate that their protoliths were spinel peridotites that were melt-depleted at shallow (1 GPa) depths. These spinel peridotites were subsequently refertilised and transported to cold and deep final conditions in the garnet stability field (Chin *et al.*, 2012, 2014). Temperatures corresponding to melting, and thus initial temperatures, can be obtained using Fe-Mg partitioning between peridotite and melt (Lee and Chin, 2014). Melting temperatures for the garnet peridotites fall between 1300 and 1400 °C (Chin *et al.*, 2012). These initial

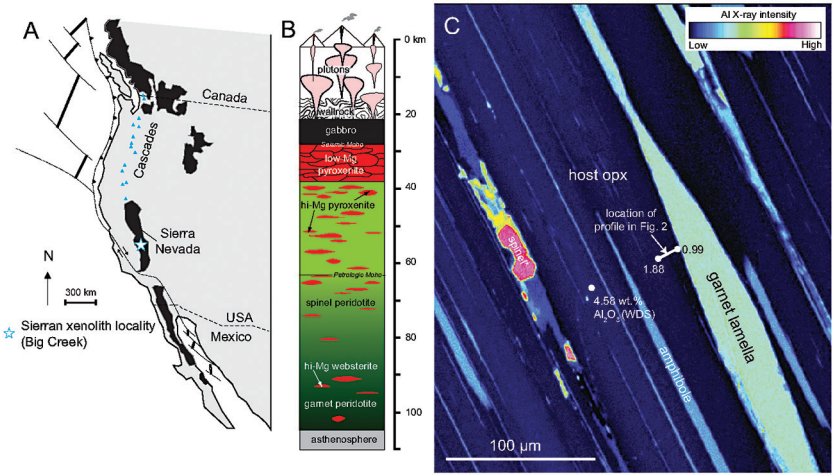

Figure 1 **(A)** Sample locality map. **(B)** Vertical architecture of the lithosphere beneath the central Sierra Nevada as sampled by xenoliths (see text for references). **(C)** Wavelength-dispersive (WDS) elemental map of Al intensity in an orthopyroxene containing garnet and amphibole lamellae in garnet peridotite 1026V from 3 GPa (~90 km). Spots labelled as wt.% Al_2O_3 correspond to individual, quantitative WDS spot measurements.

temperatures are consistent with the high Al in orthopyroxene away from contact with exsolved garnet lamellae (Fig. 1C). For example, in the profile shown in Figure 1C, the distal Al_2O_3 of 1.88 wt. % would correspond to 1275 °C at 3 GPa using the garnet-orthopyroxene thermobarometer of Harley and Green (1982).

For this study, one garnet peridotite (1026V) containing well-developed garnet exsolution lamellae was selected for modelling diffusion kinetics. Garnet pyroxenites were selected for Lu-Hf and Sm-Nd chronology owing to their high modal abundances of garnet (25–50 %) and clinopyroxene (50–60 %) (garnet peridotites provided insufficient quantities of separable garnet for dating). We chose a low-MgO pyroxenite (BCX; final T of 801 °C and final P of 0.33 GPa using the REE garnet-clinopyroxene thermobarometer of Sun and Liang (2015)), a high-MgO websterite (BC98-5, average final T of 702 °C and average final P of 2.4 GPa), and a high-MgO amphibole-bearing websterite (BC98-7, average final T of 710 °C and average final P of 1.6 GPa). Sample BC98-7 has an amphibole vein replacing pyroxene and hence was selected deliberately to provide insight into the timing of hydrous metasomatism.

Methods

High spatial resolution elemental data on sample 1026V were determined by field emission electron microprobe analyser (EPMA) using wavelength-dispersive spectroscopy (WDS) with operating conditions at 15 kV accelerating voltage and

5 nA probe current using the JEOL JXA-8530 F 'Hyperprobe' at Yale University. Core and rim mineral compositions in garnet pyroxenites were determined by WDS (15 kV, 20 nA) on the CAMECA SX-50 at Texas A&M University. Typical spot sizes on both electron probes were 1 to 1.5 µm.

Thermobarometry was based on mineral major and trace element compositions published in Lee *et al.* (2006) and Chin *et al.* (2012) and the data reported in this study.

For Sm-Nd and Lu-Hf isotopic analysis, clean garnet and clinopyroxene were separated by hand. Between 60 and 680 mg of garnet, clinopyroxene, and whole-rock powders were acid-digested in Parr bombs. Sm, Nd, Lu and Hf were separated by ion-exchange column chromatography and their isotopic compositions measured by multiple-collector inductively coupled plasma mass spectrometry following the procedures outlined in Blichert-Toft *et al.* (1997, 2002), Blichert-Toft (2001), and Blichert-Toft and Puchtel (2010). Sm, Nd, Lu and Hf concentrations were determined by isotope dilution using >98 % pure mixed ^{149}Sm-^{150}Nd and ^{176}Lu-^{180}Hf spikes added to the samples at the outset of dissolution. Data and further details of the analytical procedures are in the Supplementary Information.

Al diffusion modelling was done by finite-difference, allowing for temperature-dependent diffusivity and boundary conditions. Magnitude of time-steps were adapted with temperature and diffusivity to maintain numerical closure. Thermal modelling was based on conventional finite-difference models of conduction. Additional details on modelling set up and parameters are provided in the Supplementary Information.

Results

Al-depletion haloes in orthopyroxene. Field emission electron microprobe measurements show that BC98-7, BC98-5, and 1026V have orthopyroxenes zoned from high-Al cores to low-Al rims (Supplementary Information). In particular, Al in orthopyroxene porphyroclasts becomes depleted towards the contacts with garnet exsolution lamellae. Al-depletion halo thicknesses in orthopyroxene adjacent to the garnet lamellae range from 5-20 µm and are positively correlated with garnet lamellae thickness, confirming that garnet formed by exsolution from an original high-Al, high-temperature pyroxene (Chin *et al.*, 2012). The Al concentration profiles exhibit strong curvature due to 50 % depletion within the first ~5 µm from the contact followed by only moderate (15 %) depletion 5-20 µm from the contact (Fig. 2).

Diffusion modelling. The thickness and shape of the Al-depletion halo in garnet peridotite-hosted pyroxenes in sample 1026V can be used to constrain the cooling rate of the xenolith during its residence in the deep lithosphere. We numerically solved the 1-D chemical diffusion equation with temperature-dependent diffusivity and temperature-dependent boundary conditions at the

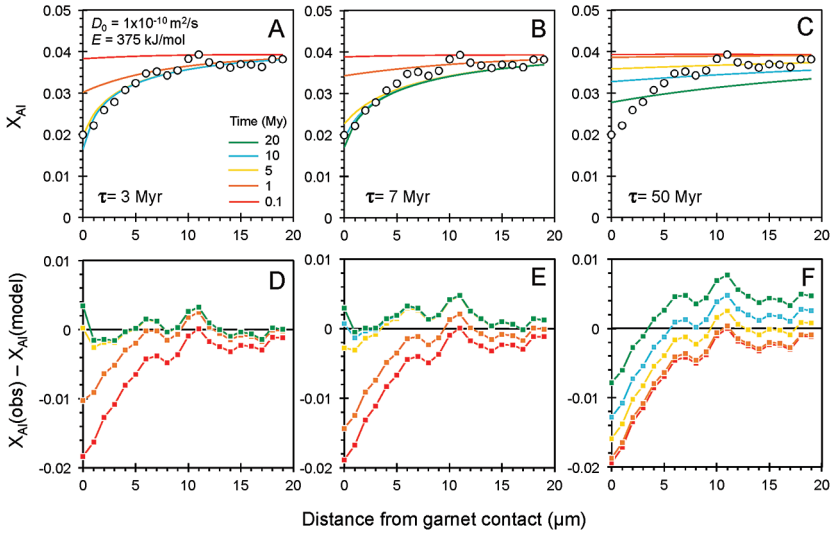

Figure 2 Orthopyroxene Al diffusion modelling of the Al halo transect shown in Figure 1C. Quantitative WDS spot analyses along the transect are plotted as white circles. **(A-C)** show diffusion profiles at selected times (0.1, 1, 5, 10, 20 Ma) using an activation energy *E* of 375 kJ/mol and D_0 = 10^{-10} m^2/s. Three different cooling scenarios are shown, with e-fold timescales of cooling τ of 3, 7, and 50 Myr. **(D-F)** show the residual (X_{Al}(observed) – X_{Al}(modelled)) as a function of distance for each of the models, where X_{Al} = atomic Al/2, and Al is the number of cations in the formula for orthopyroxene on a 6 oxygen basis.

garnet-pyroxene interface for a range of possible cooling histories (see Supplementary Information for details on the modelling approach). We assumed that cooling and associated garnet exsolution occurred isobarically at the final recorded equilibration pressures in 1026V (3 GPa). We adopted an initial temperature of 1275 °C, corresponding to the maximum Al_2O_3 content of 1.88 wt. % far from the garnet contact (Fig. 1C, Table S-1). We also explored a lower initial temperature of 1100 °C, corresponding to the high-Al cores in the high-MgO websterites to evaluate whether our chemical diffusion modelling could be used to interpret the thermal evolution of the coexisting websterites, which show similar Al zoning in orthopyroxenes. For the final temperature, we use 750 °C, corresponding to mineral rim compositions and thus final equilibration temperatures of both peridotites and websterites. To explore the range of possible cooling histories, we assumed that temperature decreased exponentially from 1275 to 750 °C over e-fold timescales τ ranging from 3, 7, and 50 Myr. The temperature-dependent boundary condition was determined by parameterising the garnet-orthopyroxene thermobarometer of Harley and Green (1982) at 3 GPa.

No experimental data are available for Al diffusion in orthopyroxene, but experiments on REE^{3+} diffusion in orthopyroxene may provide a suitable analogue for estimating the parameters of diffusivity *D*, that is, $D = D_0\exp(-E/RT)$, where D_0 is the pre-exponent (m^2/s), *E* is the activation energy (kJ/mol), *R* is the gas constant, and *T* is temperature (K). Cherniak and Liang (2007) obtained a D_0 of 1.2×10^{-7} m^2/s and *E* of 369 kJ/mol after averaging all experimental data for REE and Y diffusion in orthopyroxene. They showed that *E* does not vary with cation radius, so *E* for Al diffusivity is assumed to be similar. We therefore adopted a nominal value of 375 kJ/mol for *E* though other values are explored in the Supplementary Information. D_0, however, is expected to vary with ionic radius based on experiments on clinopyroxene (Van Orman *et al.*, 2001), but the relationship is not clear for experiments on orthopyroxene. We thus varied D_0 from 10^{-7} to 10^{-12} m^2/s over the three cooling scenarios and evaluated which combination of parameters best match the magnitude and curvature of the Al-depletion halo. For a given cooling scenario, as D_0 increases, the modelled profiles progressively flatten because the higher the D_0, the faster the Al diffusion front can propagate into the pyroxene. For a given D_0, decreasing the cooling rate decreases curvature because longer cooling times allow more time for diffusion.

In Figure 2A-C, we show model results of Al profiles, including residuals (Fig. 2D-F), versus elapsed time. The parameters used for the model results in Figure 2 were D_0 of 10^{-10} m^2/s, *E* of 375 kJ/mol, τ of 3, 7, and 50 Myr, starting temperature of 1275 °C, and final temperature of 750 °C (results of models using starting temperature of 1100 °C are shown in the Supplementary Information). The best fit models require closure of the system for Al within 5 Myr for τ of 3 Myr and within 10 Myr for τ of 7 Myr. Model results for other D_0s give poor fits or require unreasonable cooling rates to achieve a good fit. For example, the only model using D_0 of 10^{-11} m^2/s consistent with the observed Al profile requires τ of 50 Myr and closure at 100 Myr, while it is clear that a cooling duration of 100 Myr for the Sierran deep lithosphere is unacceptably long given the well-constrained magmatic peak at ~95 Ma (Paterson *et al.*, 2014) and closure of garnet websterite Sm-Nd ages between 81 and 89 Ma (discussed below). The most robust models are for D_0 of 10^{-10} m^2/s and τ of 3-7 Myr and indicate that the base of the Sierran lithosphere (90 km) cooled from 1275 to 750 °C within 10 Myr. We note that if we had assumed a lower initial temperature (1100 °C) corresponding to the maximum Al in orthopyroxene cores in the garnet websterites, we obtain a similar result consistent with cooling within 10 Myr at fast cooling rates (Supplementary Information).

Coupled Lu-Hf and Sm-Nd chronology. Additional constraints on the cooling history of the Sierran lithosphere come from coupled Lu-Hf and Sm-Nd chronology. Although the closure temperatures of the Lu-Hf and Sm-Nd systems depend on many factors, such as cooling rate, grain size, and diffusion parameters, which are not always well constrained in texturally complex systems, it is known that the Lu-Hf system closes at higher temperatures than the Sm-Nd system (Kylander-Clark *et al.*, 2007; Cheng *et al.*, 2008). The slopes of lines

regressed through garnet, clinopyroxene, and whole-rock data on $^{176}Hf/^{177}Hf$ versus $^{176}Lu/^{177}Hf$ and $^{143}Nd/^{144}Nd$ versus $^{147}Sm/^{144}Nd$ diagrams yield ages broadly coeval with magmatism (120-85 Ma) in the Sierra Nevada (Fig. 3). For the deep high-MgO websterite (BC98-5), Lu-Hf and Sm-Nd ages are identical to within analytical uncertainties (92.6 ± 1.6 Ma and 88.8 ± 3.1 Ma, respectively). For the shallow low-MgO pyroxenite (BCX), the Lu-Hf age is considerably older (107.9 ± 1.4 Ma) than the Sm-Nd age (84.0 ± 4.1 Ma), the former coinciding with the main peak of arc magmatism as inferred from the ages of plutons and the latter coinciding with the tail end of the magmatic flare-up. For the amphibole-bearing sample BC98-7, the Lu-Hf age is younger (60.8 ± 3.2 Ma) than the Sm-Nd age (81.0 ± 2.0 Ma), the latter of which is consistent within the quoted uncertainties with the Sm-Nd ages of the other samples.

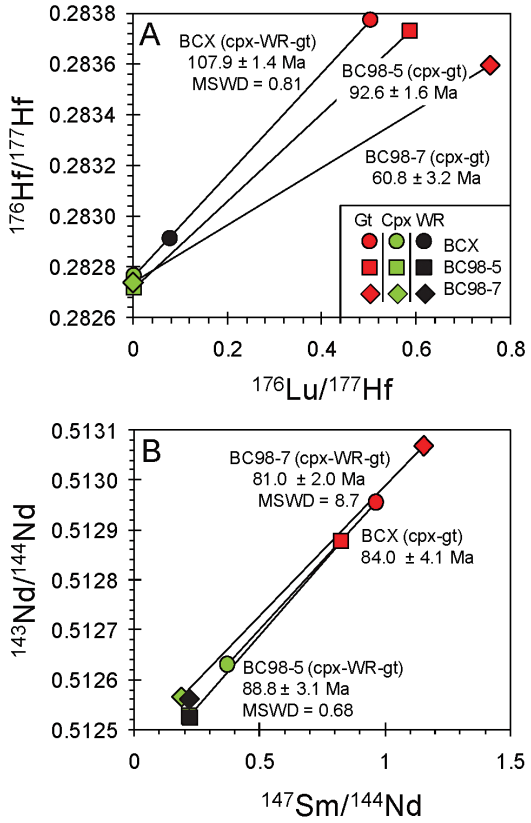

Figure 3 **(A)** Lu-Hf and **(B)** Sm-Nd isochrons of Sierran garnet pyroxenite xenoliths. Isochrons were calculated using a MatLab least-squares software by F. Albarède (version 6.0, 2013).

Discussion

The rapid cooling rates of the deep Sierran lithosphere inferred from Al-diffusion modelling are consistent with the near-identical Lu-Hf and Sm-Nd isochron ages of the deep garnet websterite BC98-5. The Lu-Hf and Sm-Nd ages of BC98-5 constrain cooling between the two closure temperatures to be within 5 Myr. Thus, diffusion modelling and chronology suggest that the base of the Sierran lithosphere remained hot until ~92 Ma (the Lu-Hf age), after which it cooled rapidly. In contrast, the coincidence of shallow pyroxenite BCX's Lu-Hf age with pluton ages suggests that the 108 Ma Lu-Hf age simply may represent a crystallisation age during passage of magmas in the cold shallow parts of the lithosphere (<45 km) (Fig. 4A, B). BCX's young Sm-Nd age, however, is identical to ages from the base of the lithosphere as represented by BC98-5, indicating that, although BCX crystallised at 108 Ma, it cooled slowly after crystallisation, passing through the Sm-Nd closure temperature at roughly the same time as the deep lithosphere as recorded by BC98-5. This suggests that the entire lithosphere, as represented by the shallow low-MgO pyroxenite and the deep high-MgO websterite and peridotites, experienced cooling at around 92 Ma, just after the peak of arc magmatism. The Lu-Hf and Sm-Nd systematics of amphibole-bearing BC98-7 from the base of the Sierran lithosphere is more perplexing because, although its Sm-Nd age of 81 Ma is within error of Sierran magmatism, its Lu-Hf age is much younger (60.8 Ma). However, we note that the chemical dissimilarity between rare earth element Lu and high field strength element Hf allows for more extreme parent/daughter fractionation in fluid-mediated processes, whereas Sm and Nd, two neighbouring light rare earth elements, are more difficult to fractionate owing to their similar chemical behaviour under all conditions. Thus, the young Lu-Hf age of BC98-7 may reflect resetting by fluid metasomatism of the deep lithosphere continuing well after arc magmatism ended.

One scenario that may explain the rapid cooling inferred at the base of the Sierran lithosphere is if the lithosphere impinged against a cold subducting plate. To satisfy the age constraints, such impingement would have had to occur at ~92 Ma and the depth at which the impingement occurred must have been greater than the deepest xenolith equilibration pressures of ~3 GPa (~100 km). To simulate this scenario, we modelled thermal diffusion in a 100-km thick lithosphere that is instantaneously juxtaposed against a cold slab at 100 km depth. We assume the deepest part of the Sierran lithosphere, represented by interleaved high-MgO garnet websterite and garnet peridotite, to be initially 1300 °C, decreasing with decreasing depth to a surface temperature of 25 °C. We take the temperature of the top of a slab to be 750 °C, based on Syracuse *et al.* (2010). Cooling histories are shown in Figures 4C and 4D, where it can be seen that the deepest part of the lithosphere cools the fastest. In Figure 4D, the cooling histories determined from Al-diffusion kinetics, using 1275 °C as the initial temperature and 750 °C as the final temperature (Fig. 2), are also compared with the cooling histories from the conductive cooling model. Thus, Al-diffusion kinetics, coupled Sm-Nd

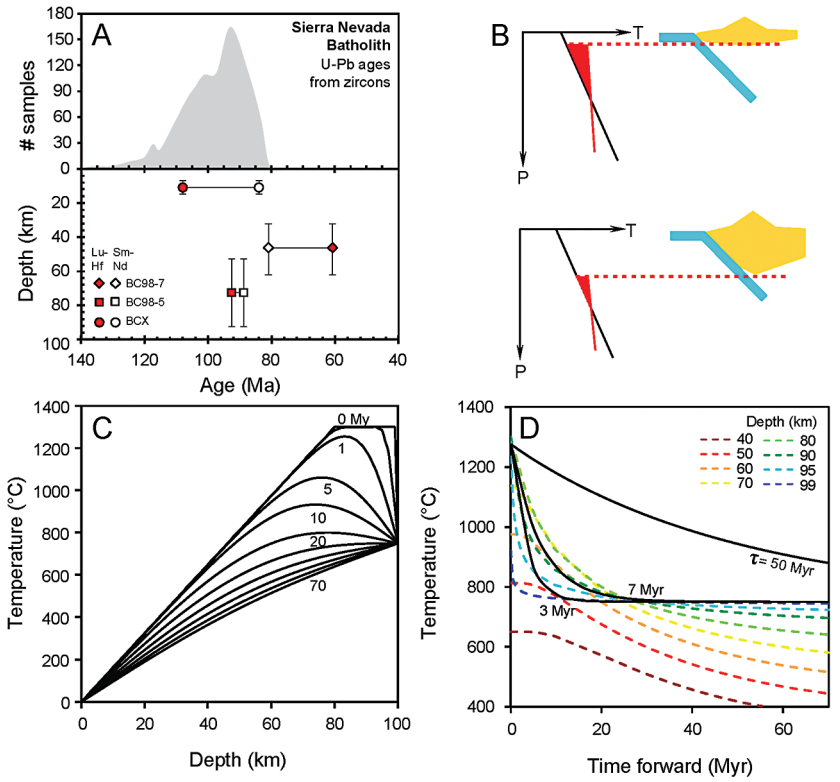

Figure 4 **(A) Top panel:** U-Pb zircon ages from the Sierra Nevada Batholith (Paterson *et al.*, 2014) showing a major peak at ~95 Ma. **Bottom panel:** Thermobarometrically constrained depth versus radiometric age of Sierran pyroxenite xenoliths. The vertical bars represent the range of final P, T recorded by several mineral rim pairs in each xenolith (except for BCX, where average REE concentrations were used); the symbols represent the average P, T. **(B)** Cartoon illustrating the formation of shallow low-MgO pyroxenite (top) and deep high-MgO websterite (bottom). **(C)** Temperature versus depth diagram showing the initial condition of conductive cooling modelling of a 100-km thick lithosphere at 0 Myr (initial condition) and re-equilibration to a new ambient geotherm after 70 Myr. Thermal diffusivity is 10^{-6} m^2/s. **(D)** Temperature versus time diagram of depth slices ranging from 40 to 99 km. Superimposed on the diagram are the three cooling scenarios evaluated in the Al-diffusion modelling.

and Lu-Hf chronology, and thermal modelling all independently lead to the same conclusion that the base of the Sierran lithosphere cooled from >1250 °C to 750 °C in <10 Myr, just after the peak of arc magmatism.

Although cooling of the deep Sierran lithosphere by slab "refrigeration" has been suggested previously, shallowing of the slab dip typically has been invoked (Dickinson and Snyder, 1978; Dumitru *et al.*, 1991). However, the presence of

cold xenoliths at ~100 km depth requires, instead, that the Sierran arc lithosphere thickened downward and impinged upon a normally dipping slab, ~100 km beneath the arc front. The coincidence of thickening with the peak of arc magmatism suggests that crustal thickening must have, in part, been driven by magmatic additions to the crust (Flowers *et al.*, 2005; Jagoutz, 2010). We therefore propose that magmatic thickening may be a key mechanism that modulates the tempo of arc magmas, specifically the abrupt cessation of magmatism observed in many continental arcs. With progressive magmatic additions to the crust, the upper plate thickens, eventually impinging against the cold subducting lower plate and terminating magmatism. In other words, magmatic flare-ups, whatever their origin, cannot be sustained for long periods of time if magmatism leads to thickening. The ability for magmatism to thicken the upper plate depends on the stress state of the upper plate (Karlstrom *et al.*, 2014). In many island arcs, the upper plate is in extension, which could compensate for magmatic thickening. In contrast, the upper plate in continental arcs tends to be in compression, adding to the effects of magmatic thickening (DeCelles, 2004; Paterson *et al.*, 2011). Because of these intimate relationships between magmatism and crustal thickness, we predict that continental arc magmatism should rise and fall over tens of millions of years, while magmatism in island arcs should be long-lived.

Acknowledgements

We thank Simon Harley and Chenguang Sun for thorough and critical reviews. We also thank Wenrong Cao and Scott Paterson for insightful discussions while writing the manuscript. This work was supported by the US-NSF grant EAR-1119315 to C.-T.A. Lee, a Geological Society of America Grant-in-Aid and the Martha Lou Broussard Fellowship to E.J. Chin, and the French Agence Nationale de la Recherche grant ANR-10-BLAN-0603 (M&Ms – Mantle Melting – Measurements, Models, Mechanisms) to J. Blichert-Toft.

Editor: Bruce Watson

Additional Information

Supplementary Information accompanies this letter at http://www.geochemicalperspectivesletters.org/article1503

Reprints and permission information is available online at http://www.geochemicalperspectivesletters.org/copyright-and-permissions

Cite this letter as: Chin, E.J., Lee, C.-T.A., Blichert-Toft, J. (2015) Growth of upper plate lithosphere controls tempo of arc magmatism: Constraints from Al-diffusion kinetics and coupled Lu-Hf and Sm-Nd chronology. *Geochem. Persp. Let.* 1, 20-32.

Author Contributions

E.J. Chin collected the electron microprobe data; J. Blichert-Toft and E.J. Chin did the Lu-Hf and Sm-Nd isotope measurements; E.J. Chin and C.-T.A. Lee modelled the Al and thermal diffusion; and E.J. Chin wrote the manuscript with help from C.-T.A. Lee and J. Blichert-Toft. All authors discussed the results and commented on the manuscript.

References

Barton, M.D. (1996) Granitic magmatism and metallogeny of southwestern North America. In: Brown, M., Candela, P.A., Peck, D.L., Stephens, R.J.W., Zen, E.-A. (Eds.) *The Third Hutton Symposium on the Origin of Granites and Related Rocks*. GSA Special Papers, 261-280.

Blichert-Toft, J. (2001) On the Lu-Hf Isotope Geochemistry of Silicate Rocks. *Geostandards Newsletter* 25, 41-56.

Blichert-Toft, J., Puchtel, I.S. (2010) Depleted mantle sources through time: Evidence from Lu-Hf and Sm-Nd isotope systematics of Archean komatiites. *Earth and Planetary Science Letters* 297, 598-606.

Blichert-Toft, J., Chauvel, C., Albarède, F. (1997) Separation of Hf and Lu for high-precision isotope analysis of rock samples by magnetic sector-multiple collector ICP-MS. *Contributions to Mineralogy and Petrology* 127, 248-260.

Blichert-Toft, J., Boyet, M., Télouk, P., Albarède, F. (2002) $^{147}Sm/^{143}Nd$ and $^{176}Lu/^{176}$ Hf in eucrites and the differentiation of the HED parent body. *Earth and Planetary Science Letters* 204, 167-181.

Cheng, H., King, R.L., Nakamura, E., Vervoort, J.D., Zhou, Z. (2008) Coupled Lu–Hf and Sm–Nd geochronology constrains garnet growth in ultra-high-pressure eclogites from the Dabie orogen. *Journal of Metamorphic Geology* 26, 741-758.

Cherniak, D.J., Liang, Y. (2007) Rare earth element diffusion in natural enstatite. *Geochimica et Cosmochimica Acta* 71, 1324-1340.

Chin, E.J., Lee, C.-T.A., Luffi, P., Tice, M. (2012) Deep Lithospheric Thickening and Refertilization beneath Continental Arcs: Case Study of the P, T and Compositional Evolution of Peridotite Xenoliths from the Sierra Nevada, California. *Journal of Petrology* 53, 477-511.

Chin, E.J., Lee, C.-T.A., Barnes, J.D. (2014) Thickening, refertilization, and the deep lithosphere filter in continental arcs: Constraints from major and trace elements and oxygen isotopes. *Earth and Planetary Science Letters* 397, 184-200.

Coleman, D.S., Glazner, A.F. (1997) The Sierra Crest Magmatic Event: Rapid Formation of Juvenile Crust during the Late Cretaceous in California. *International Geology Review* 39, 768-787.

DeCelles, P.G. (2004) Late Jurassic to Eocene evolution of the Cordilleran thrust belt and foreland basin system, western U.S.A. *American Journal of Science* 304, 105-168.

DeCelles, P.G., Ducea, M.N., Kapp, P., Zandt, G. (2009) Cyclicity in Cordilleran orogenic systems. *Nature Geoscience* 2, 251-257.

Dickinson, W.R., Snyder, W.S. (1978) Plate tectonics of the Laramide orogeny. In: Matthews, V. (Ed.) *Laramide folding associated with basement block faulting in the Western United States*. Geological Society of America Memoir 151, 355-366.

Dodge, F.C.W., Lockwood, J.P., Calk, L.C. (1988) Fragments of the mantle and crust from beneath the Sierra Nevada batholith: Xenoliths in a volcanic pipe near Big Creek, California. *Geological Society of America Bulletin* 100, 938-947.

Ducea, M.N. (2001) The California Arc: Thick Granitic Batholiths, Eclogitic Residues, Lithospheric-Scale Thrusting, and Magmatic Flare-Ups. *GSA Today* 11, 4-10.

Ducea, M.N., Saleeby, J.B. (1996) Buoyancy sources for a large, unrooted mountain range, the Sierra Nevada, California: Evidence from xenolith thermobarometry. *Journal of Geophysical Research* 101, 8229-8244.

Ducea, M.N., Saleeby, J.B. (1998) The age and origin of a thick mafic–ultramafic keel from beneath the Sierra Nevada batholith. *Contributions to Mineralogy and Petrology* 133, 169-185.

Dumitru, T.A., Gans, P.B., Foster, D.A., Miller, E.L. (1991) Refrigeration of the western Cordilleran lithosphere during Laramide shallow-angle subduction. *Geology* 19, 1145-1148.

Flowers, R.M., Bowring, S.A., Tulloch, A.J., Klepeis, K.A. (2005) Tempo of burial and exhumation within the deep roots of a magmatic arc, Fiordland, New Zealand. *Geology* 33, 17-20.

Harley, S.L., Green, D.H. (1982) Garnet-orthopyroxene barometry for granulites and peridotites. *Nature* 300, 697-701.

Haschke, M., Siebel, W., Günther, A., Scheuber, E. (2002) Repeated crustal thickening and recycling during the Andean orogeny in north Chile (21-26 S). *Journal of Geophysical Research: Solid Earth (1978-2012)* 107, ECV 6-1-ECV 6-18.

Jagoutz, O. (2010) Construction of the granitoid crust of an island arc. Part II: a quantitative petrogenetic model. *Contributions to Mineralogy and Petrology* 160, 359-381.

Karlstrom, L., Lee, C.-T.A., Manga, M. (2014) The role of magmatically driven lithospheric thickening on arc front migration. *Geochemistry, Geophysics, Geosystems* 15, 2655-2675.

Kay, S.M., Coira, B.L. (2009) Shallowing and steepening subduction zones, continental lithospheric loss, magmatism, and crustal flow under the Central Andean Altiplano-Puna Plateau. *Backbone of the Americas: shallow subduction, plateau uplift, and ridge and terrane collision* 204, 229-259.

Kylander-Clark, A.R., Hacker, B.R., Johnson, C.M., Beard, B.L., Mahlen, N.J., Lapen, T.J. (2007) Coupled Lu-Hf and Sm-Nd geochronology constrains prograde and exhumation histories of high-and ultrahigh-pressure eclogites from western Norway. *Chemical Geology* 242, 137-154.

Lee, C.-T.A., Chin, E.J. (2014) Calculating melting temperatures and pressures of peridotite protoliths: Implications for the origin of cratonic mantle. *Earth and Planetary Science Letters* 403, 273-286.

Lee, C.-T.A., Cheng, X., Horodyskyj, U. (2006) The development and refinement of continental arcs by primary basaltic magmatism, garnet pyroxenite accumulation, basaltic recharge and delamination: insights from the Sierra Nevada, California. *Contributions to Mineralogy and Petrology* 151, 222-242.

Lee, C.-T.A., Morton, D.M., Kistler, R.W., Baird, A.K. (2007) Petrology and tectonics of Phanerozoic continent formation: From island arcs to accretion and continental arc magmatism. *Earth and Planetary Science Letters* 263, 370-387.

Mukhopadhyay, B., Manton, W.I. (1994) Upper-Mantle Fragments from Beneath the Sierra Nevada Batholith: Partial Fusion, Fractional Crystallization, and Metasomatism in a Subduction Related Ancient Lithosphere. *Journal of Petrology* 35, 1417-1450.

Paterson, S.R., Okaya, D., Memeti, V., Economos, R., Miller, R.B. (2011) Magma addition and flux calculations of incrementally constructed magma chambers in continental margin arcs: Combined field, geochronologic, and thermal modeling studies. *Geosphere* 7, 1439-1468.

Paterson, S.R., Memeti, V., Anderson, L., Cao, W., Lackey, J.S., Putirka, K.D., Miller, R.B., Miller, J.S., Mundil, R. (2014) Day 6: Overview of arc processes and tempos. *Field Guides* 34, 87-116.

Pilger, R.H. (1984) Cenozoic plate kinematics, subduction and magmatism: South American Andes. *Journal of the Geological Society* 141, 793-802.

Saleeby, J., Ducea, M., Clemens-Knott, D. (2003) Production and loss of high-density batholithic root, southern Sierra Nevada, California. *Tectonics* 22, 1064.

Sun, C., Liang, Y. (2015) A REE-in-garnet-clinopyroxene thermobarometer for eclogites, granulites and garnet peridotites. *Chemical Geology* 393-394, 79-92.

Syracuse, E.M., van Keken, P.E., Abers, G.A. (2010) The global range of subduction zone thermal models. *Physics of the Earth and Planetary Interiors* 183, 73-90.

Van Orman, J., Grove, T., Shimizu, N. (2001) Rare earth element diffusion in diopside: influence of temperature, pressure, and ionic radius, and an elastic model for diffusion in silicates. *Contributions to Mineralogy and Petrology* 141, 687-703.